ACS APPLIED MATERIALS & INTERFACES

Research Article

www.acsami.org

An Effective Integrated Design for Enhanced Cathodes of Ni Foam-Supported Pt/Carbon Nanotubes for Li-O_2 Batteries

Jiaxin Li,[†,‡] Yi Zhao,[†] Mingzhong Zou,[‡] ChuXin Wu,[†] Zhigao Huang,*[,‡] and Lunhui Guan*[,†,§]

[†]State Key Laboratory of Structural Chemistry, Fujian Institute of Research on the Structure of Matter, Chinese Academy of Sciences, Fuzhou 350002, China

[‡]College of Physics and Energy, Fujian Normal University, Fuzhou 350007, China

[§]Key Laboratory of Design and Assembly of Functional Nanostructures, Chinese Academy of Sciences, Fuzhou 350002, China

Supporting Information

ABSTRACT: Designing an effective microstructural cathode combined with a highly efficient catalyst is essential for improving the electrochemical performance of Li-O_2 batteries (LOBs), especially for long-term cycling. We present a nickel foam-supported composite of Pt nanoparticles (NPs) coated on self-standing carbon nanotubes (CNTs) as a binder-free cathode for LOBs. The assembled LOBs can afford excellent electrochemical performance with a reversible capacity of 4050 mAh/g tested at 20 mA/g and superior cyclability for 80 cycles with a limited capacity of 1500 mAh/g achieved at a high current density of 400 mA/g. The capacity corresponds to a high energy density of ~3000 Wh/kg. The improved performance should be attributed to the excellent catalytic activity of highly dispersed Pt NPs, facile electron transport via loose CNTs connected to the nickel foam current collector, and fast O_2 diffusion through the porous Pt/CNTs networks. In addition, some new insights from impedance analysis have been proposed to explain the enhanced mechanism of LOBs.

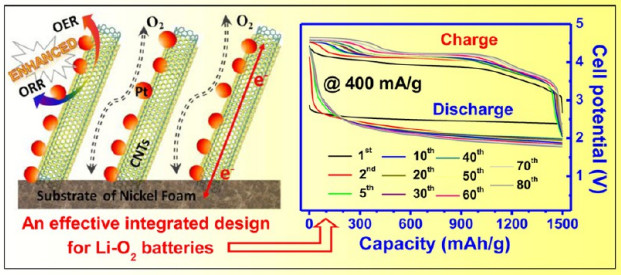

KEYWORDS: *Li-O_2 batteries, Pt/CNTs-NF cathodes, electrochemical performance, synergistic effect*

INTRODUCTION

Nonaqueous Li-O_2 batteries (LOBs) have received a heightened level of attention because of their high theoretical energy, which is almost 1 order of magnitude higher than that of the current lithium ion batteries.[1] During discharge, O_2 is reduced by electrons and combines with the Li^+ to form the product Li_2O_2, with the process being reversed on charging to release O_2 and Li^+. To make LOBs suitable for practical applications, the foremost challenge is how to allow the "$2Li^+ + 2e^- + O_2 \leftrightarrow Li_2O_2$" reaction to be reversible.[2−4] There have been extensive studies of the effects of many key factors on the reversible reaction of the O_2 electrode; these factors include catalysts, carbon active materials, cathode formulations, and the physical properties of the cathode.[5−8]

It is well-known that an ideal cathode catalyst can facilitate a complete reversibility of oxygen reduction reactions (ORRs) and oxygen evolution reactions (OERs) with low polarization for LOBs. The low polarization will reduce their discharging and charging overpotentials and further increase their round-trip energy efficiency. Tremendous effort has been devoted to developing cathode catalysts, such as functional doped-carbon materials,[9,10] metal oxides,[11−13] metal nitrides,[14,15] precious metals,[16−18] etc. Likewise, another perovskite $La_{0.75}Sr_{0.25}MnO_3$ material,[19] nonprecious iron−nitrogen−carbon (Fe/N/C),[20] and transition bimetallic nitrides (Co_3Mo_3N)[21] were reported in LOBs and showed high reversible capacities with lower ORR and OER overpotentials. Very recently, the nanoporous gold directly as the cathode without any carbon materials delivered an excellent electrochemical performance.[22] With regard to precious metals, Pt-based catalysts, including mesoporous carbon nitride loaded with Pt nanoparticles (NPs),[23] carbon-supported Pt−Au alloys,[24] and Pt nanoparticle−graphene nanosheet hybrids,[25] have also attracted a great deal of interest because of their high catalytic activity. Moreover, the related reports have pointed out that the cathode catalysts in LOBs with a nanostructural shape, a large surface area, and good conductivity can exhibit high catalytic reactivity.[26−28]

In addition to those strategies for searching for suitable catalysts and synthesis routes, developing new cathode architectures is also important and in demand. Typical cathodes for LOBs are made by using a slurry of carbon active materials, a polymeric binder, and a solvent cast onto a current collector. Correspondingly, most of the catalytic sites and diffusion pathways for O_2 and the electrolyte will be gradually blocked by the solid discharging products (Li_2O_2), further leading to a serious deterioration of their battery performance.[29] Recently,

Received: April 21, 2014
Accepted: July 10, 2014
Published: July 10, 2014

binder-free electrode design, such as the carbon-based paper electrode[30,31] and Ni foam-supported N-doped carbon nanotubes (CNTs),[32] has been demonstrated as a promising solution for the fabrication of high-energy storage devices. As a typical example, Yang's group has reported that ceramic porous substrate-supported carbon fibers as the cathode in LOBs can exhibit obviously enhanced performance.[33] Their high gravimetric energy can be attributed to low carbon packing in electrodes, the highly efficient utilization of the available carbon mass, and the void volume for Li_2O_2 formation.

To a certain extent, the performance of LOBs can be further improved by fabricating a cathode with an effective microstructure. It is believed that the good LOB cathode should possess many exciting characteristics, including a large surface area, high electrical conductivity, and strong electrocatalytic activity to the ORRs and OERs, thereby significantly improving the specific mass capacity and the cycling performance for potential practical LOBs. In that case, developing an effective method for simultaneously integrating those strategies to achieve excellent LOB performance is strongly desired. In this study, binder-free nickel foam-supported self-standing composites of Pt/CNTs have been prepared by a chemical vapor deposition method coupled with magnetic sputtering and evaluated as cathodes for LOBs (as briefly shown in Scheme 1).

Scheme 1. Configuration of the Pt/CNTs-NF Electrode

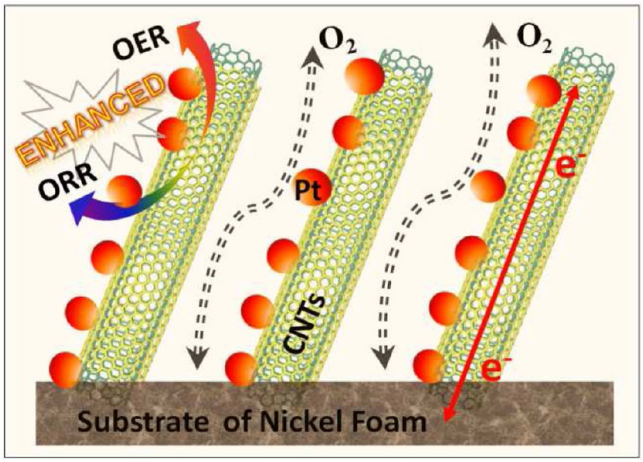

The assembled batteries can afford excellent electrochemical performance. In addition, we systematically investigate the effects of electrode fabrication on electrochemical performance by morphology and impedance analysis and further propose some new insights into the design of CNT-based electrodes for LOBs.

EXPERIMENTAL SECTION

Synthesis of Materials. The nickel foam was purchased from Changsha Liyuan Port (Changsha, China). In a typical chemical vapor deposition (CVD) experiment, the Ni foam (4 cm × 4 cm) was dipped in 2 M HCl for 10 min to remove part of the metal oxides coated on the surface of the Ni foam. After being washed with deionized water and dried, the Ni foam was put in the quartz tube and heated to 750 °C. A flow of 10% H_2 in Ar was introduced to deoxidize the coating layer. After 10 min, 20% CH_4 in an Ar flow was added to the CVD process. The growth time was 20 min. After the CVD process, the furnace was cooled to room temperature in ambient Ar. Subsequently, the Pt NPs were deposited by a dc magnetic sputtering method by using a Pt target. The Pt NPs were deposited under a 1.0 Pa Ar atmosphere with a floating rate of 20 sccm, along with a power of 60 W for 50 S. As shown in Scheme 1, the obtained product is a Pt/CNTs-Ni foam electrode (denoted as Pt/CNTs-NF electrode).

Characterization of Materials. The structure and morphology of the samples were characterized by X-ray diffraction (XRD) (RIGAKU SCXmini), Raman spectroscopy (Renishaw, excitation at 514.5 nm), energy dispersive X-ray spectroscopy (EDS), scanning electron microscopy (SEM) (JSM-6700F), and transmission electron microscopy (TEM) (Tecnai G2 F20).

Electrochemical Measurements. According to our previous report,[2] the electrochemical behaviors were measured in a Swagelok cell with a 0.5 cm^2 hole placed on the cathode side to allow the inward flow of oxygen. All the cells were assembled in a dry argon-filled glovebox. First, the obtained product was cut into a 0.8 cm^2 disk and utilized in LOBs without any additional binders or catalysts. The typical loading of the CNTs and Pt/CNTs for CNTs-NF and the Pt/CNTs-NF electrode was ~0.9 mg/cm^2. For comparison, typical CNT-coated electrodes for LOBs were prepared. The CNTs were purchased from Shenzhen Nanotech Port (Shenzhen, China) and used as received. The cathodes were prepared by casting the slurry mixtures of 90 wt % CNTs and 10 wt % polyvinylidene difluoride (PVDF) onto a nickel foam current collector. The air electrode disk also had an area of 0.8 cm^2. The typical loading of the CNTs was 0.9 ± 0.1 mg/cm^2. Then a commercially available electrolyte solution of 1 M LITFSI [lithium bis(trifluoromethanesulfonyl) imide] in TEGDME (tetraethylene glycol dimethyl ether) was impregnated into a glass fiber membrane and the membrane sandwiched between a lithium metal anode and air cathode. The batteries were cycled by LAND 2001A at room temperature with a lower voltage limit of 2.0 V and an upper limit of 4.20 V versus Li^+/Li under different conditions after a 2−3 h rest period. Cyclic voltammetry (CV) tests were conducted on a CHI660D Electrochemical Workstation at a rate of 0.20 mV/s. Electrochemical impedance spectroscopy (EIS) was conducted by applying an ac voltage of 5 mV over the frequency range from 1 mHz to 100 kHz.

RESULTS AND DISCUSSION

SEM and TEM were employed to study the structure and morphology of the samples. As shown in panels a and b of Figure 1, the skeleton of the Ni substrate is uniformly coated with interconnected CNTs. After the deposition of Pt NPs, a similar result can also be found from SEM images shown in panels a and b of Figure S1 of the Supporting Information. The opening of the three-dimensional entangled structure of the CNTs or Pt/CNTs throughout the entire electrode depth is beneficial to the fast O_2 diffusion and migration of the electron, thereby improving the electrochemical performance of electrodes for LOBs. Figure 1c shows typical TEM and high-resolution transmission electron microscopy (HR-TEM) images of CNTs. The diameter of CNTs ranges from 20 to 30 nm. For Pt/CNTs, TEM image shows that Pt NPs are well-coated on the surface of the CNTs. The interlayer spacings of 0.23 and 0.20 nm, corresponding to the (111) and (200) planes of Pt, respectively, could be found in the HR-TEM image (insets of Figure 1d and Figure S2 of the Supporting Information). The corresponding selected area electron diffraction pattern (Figure S3 of the Supporting Information) demonstrates the crystalline nature of Pt NPs. The diffraction rings are related to their (111), (200), and (311) planes. In addition, Figure S4 of the Supporting Information presents typical EDS spectra of Pt/CNTs, confirming the presence of Pt. The signal of Cu in the EDS spectra came from the holder.

The electrochemical performance of CNTs-NF and Pt/CNTs-NF electrodes was examined in Li-O_2 batteries. The initial discharge−charge (D−C) curves for both CNTs-NF and Pt/CNTs-NF electrodes are depicted in Figure 2a. The discharge capacities of the CNTs-NF and Pt/CNTs-NF

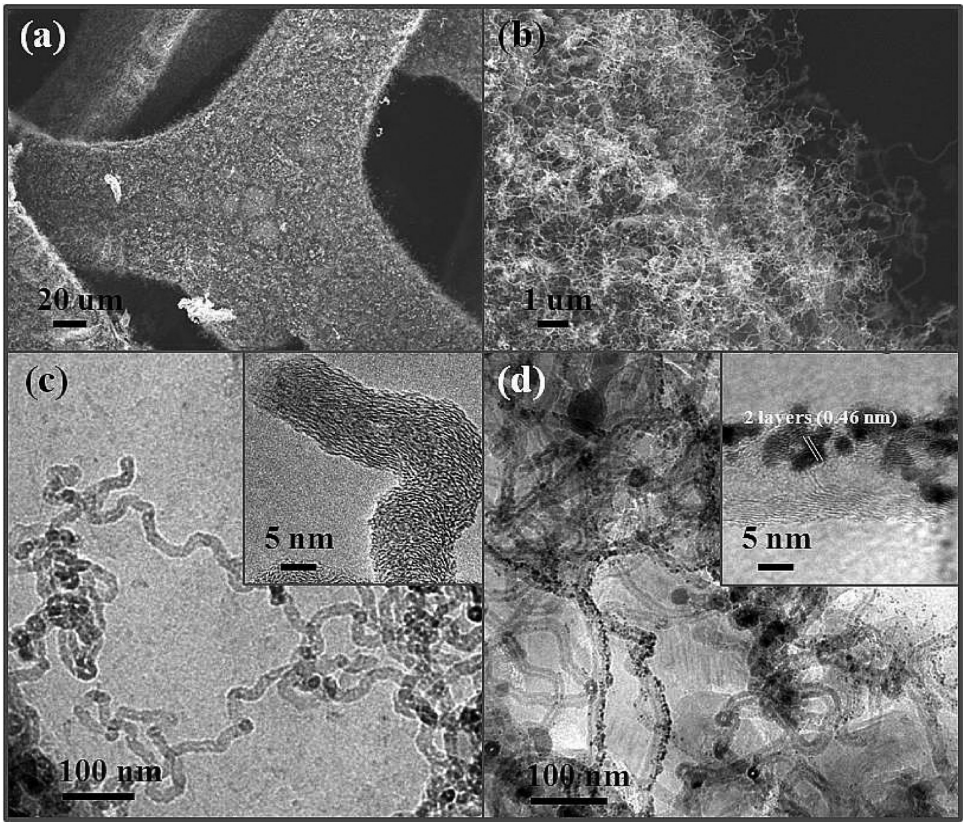

Figure 1. Microstructural analysis of CNTs-NF and Pt/CNTs-NF electrodes: (a and b) SEM images of CNTs-NF, (c) TEM image of CNTs, and (d) TEM image of Pt/CNTs (insets show HR-TEM images).

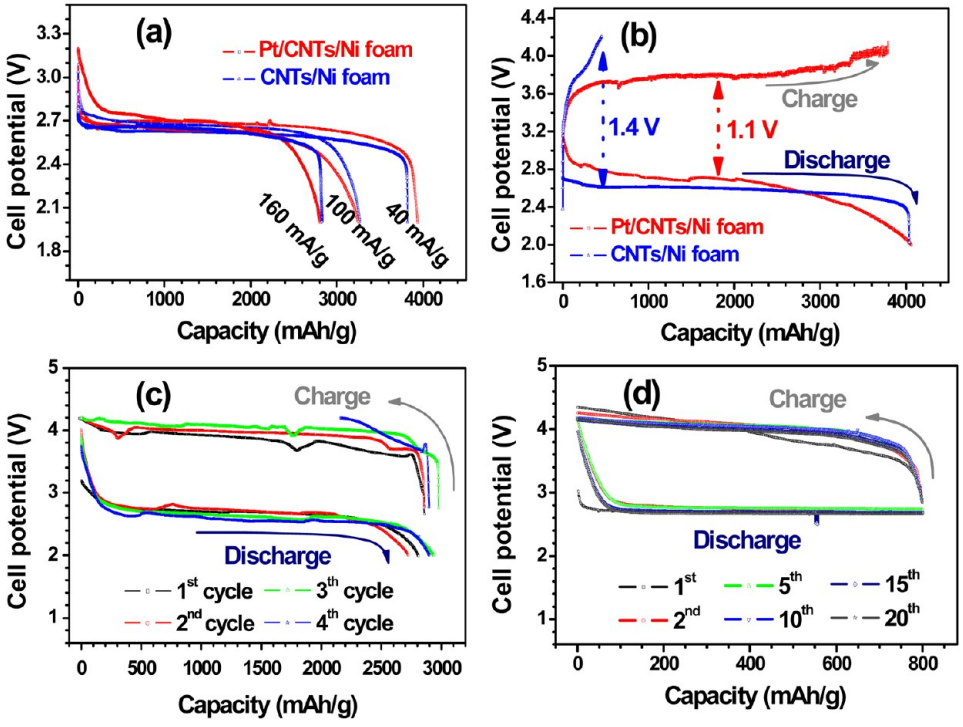

Figure 2. (a) Initial discharge−charge curves of CNTs-NF and Pt/CNTs-NF electrodes. (b) Discharge characteristics of the CNTs-NF and Pt/CNTs-NF electrodes at various current densities. (c) Discharge−charge curves of the Pt/CNTs-NF electrode at different cycles. (d) Cycling performance of the Pt/CNTs-NF electrode at 160 mA/g with the capacity curtailed to 800 mAh/g.

electrodes were 4040 and 4050 mAh/g, respectively. However, the charging capacity for the CNTs-NF electrode is much lower than that of the Pt/CNTs-NF electrode, indicating that the D−C process for the CNTs-NF electrode without the Pt catalyst is

almost irreversible. In addition, the potential difference between the charging and discharging of the Pt/CNTs-NF electrode was 1.1 V, significantly lower than the value of 1.4 V of the CNTs-NF electrode. The results confirm the catalytic effect of Pt NPs in the ORR−OER process for LOBs. Presumably, the ORR catalytic activity of Pt NPs leads to the promotion of the formation of the discharging product near the active site of the catalyst, followed by formation on the carbon surface.[14,21] Moreover, the results are consistent with the CV results for these two samples (shown in Figure S5 of the Supporting Information). Likewise, the Raman result shown in Figure S6 of the Supporting Information reveals that the Pt/CNTs-NF electrode could allow the "$2Li^+ + 2e^- + O_2 \leftrightarrow Li_2O_2$" reaction to remain reversible.[34] Figure 2b displays the initial discharge curves of CNTs-NF and Pt/CNTs-NF electrodes at 40, 100, and 160 mA/g. Interestingly, these two electrodes show similar first discharging capacities at their corresponding current densities. For comparison, typical CNT-coated electrodes for LOBs were prepared and investigated. As shown in Figure S7 and Table S1 of the Supporting Information, the batteries discharged at 20 and 160 mA/g can deliver capacities of 3205 and 1265 mAh/g, respectively, resulting in a capacity loss of ∼60%. By contrast, with the increase in discharging current densities, both CNTs-NF and Pt/CNTs-NF electrodes show a much lower capacity loss of ∼30% [i.e., (4050 − 2820)/4050 = 30%]. The improved performance should be attributed to the enhanced conductivity and unique architecture of CNTs-NF and Pt/CNTs-NF electrodes. The related enhanced mechanism has been tentatively studied in the last analysis part of Figure 5 and Figures S15 and S16 of the Supporting Information.

The D−C voltage profiles of the Pt/CNTs-NF electrode at various cycles at a current density of 160 mA/g between 2.0 and 4.2 V are presented in Figure 2c. Its discharge capacity stabilizes at ∼2900 mAh/g on the first four cycles at a deep discharge to 2.0 V. The LOB was found to exhibit an increasing capacity in those initial three cycles because of a gradual activation mechanism.[14] The activation process is favorable for the improvement of electrochemical kinetics. Although the fourth charging process stopped at 4.2 V and delivered a low capacity of only ∼830 mAh/g, it does not mean that the Pt/CNTs-NF electrodes fail to possess excellent performance, especially for cycling with a given restricting capacity. Figure 2d shows the cycling performance of the Pt/CNTs-NF electrode at 160 mA/g with a restricting capacity of 800 mAh/g. It is found that their D−C plateaus for the first cycle were ∼2.7 and ∼4.0 V, revealing its reasonable round-trip efficiency. Interestingly, the potential plateaus stay at a constant level in the following 19 cycles, indicating a stable reversible process.

To further investigate the excellent performance of the Pt/CNTs-NF electrode, the battery was cycled with a higher restricting capacity of 1500 mAh/g at a higher current density of 400 mA/g. As anticipated, the Pt/CNTs-NF electrode demonstrated superior cycle stability up to 80 cycles (shown in Figure 3). Meanwhile, their D−C plateaus for the first cycle are ∼2.5 and ∼4.0 V, while those values are ∼2.0 and ∼4.2 V, respectively, in the following 79 cycles (shown in Figure S8 of the Supporting Information). Correspondingly, its energy density is ∼3000 Wh/kg.[35] As shown in Table S2 of the Supporting Information, the obtained results are comparable with some of the latest results for LOBs.[23,24,36−40]

To understand the excellent electrochemical performance of Pt/CNTs-NF, we decomposed the batteries after different cycling stages and analyzed the morphology by SEM. The

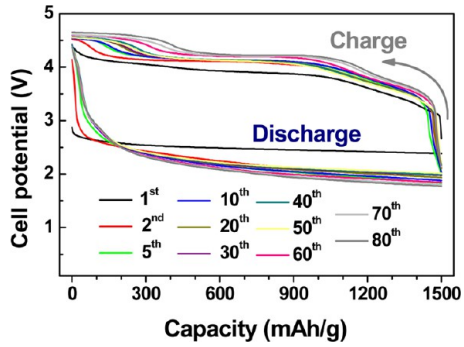

Figure 3. Cycling performance of the Pt/CNTs-NF electrode at 400 mA/g with a restricting capacity of 1500 mAh/g.

magnified SEM images of the Pt/CNTs-NF electrode after the 21th discharging state at 160 mA/g with a restricting capacity of 800 mAh/g are shown in panels a and b of Figure 4. From the SEM observation, it can be seen that the surface of the electrode contains numerous uniform nanorods, and their diameter ranges from 50 to 150 nm. In addition, Figure 4b and Figure S9 of the Supporting Information show that the discharging products were distributed on the CNTs forming as nanorods; this feature was distinguished from the fresh Pt/CNTs-NF electrode before the D−C test. Although this step ended with the discharging process, the interspace between nanorods and some roots of CNTs covered by thin products can be clearly observed. The related details for TEM observation are shown in Figures S10 and S11 of the Supporting Information. This structure not only can promote the flow of O_2 and infiltration of the electrolyte and provide enough void volume for product deposition but also can improve its conductivity. As presented in panels c and d of Figure 4, even when tested at a higher current density of 400 mA/g and a restricting capacity of 1500 mAh/g, with more discharged products deposited on the surface of the electrode, the Pt/CNTs-NF electrode presents sufficient pores between product agglomerates. These pores can also facilitate O_2 diffusion and electrolyte impregnation. Meanwhile, the aggregated products were found on the tip of entangled CNTs, and the shape of CNTs coated with Li_2O_2 products can be clearly observed. Combined with the XPS results shown in Figures S12−S14 of the Supporting Information, the observed D−C products are believed to be Li_2O and Li_2O_2, intermingled with some Li_2CO_3.[4,41−43] On the basis of Figure 4, we confirm that this unique structure of the Pt/CNTs-NF electrode can effectively enhance the conductivity of the electrode and eventually facilitate their LOB performance (as supported by the EIS results shown in panels a and b of Figure S16 of the Supporting Information).

To further confirm the standpoint mentioned above, the SEM observation of different electrodes after different D−C states was conducted, and both EIS spectra and the corresponding equivalent circuit were analyzed in detail (shown in Figures S15 and S16 of the Supporting Information). From Figure S15 of the Supporting Information, both Pt/CNTs-NF and CNTs-NF electrodes after long D−C cycles consisted of loose discharging products held in an interconnected CNT net, while that of the CNT-coated electrode delivered a compact discharging layer split from the nickel foam substrate. Moreover, some almost CNTs in the Pt/CNTs-NF electrode (shown in panels g and j of Figure S15 of the Supporting Information) can facilitate its conductivity.

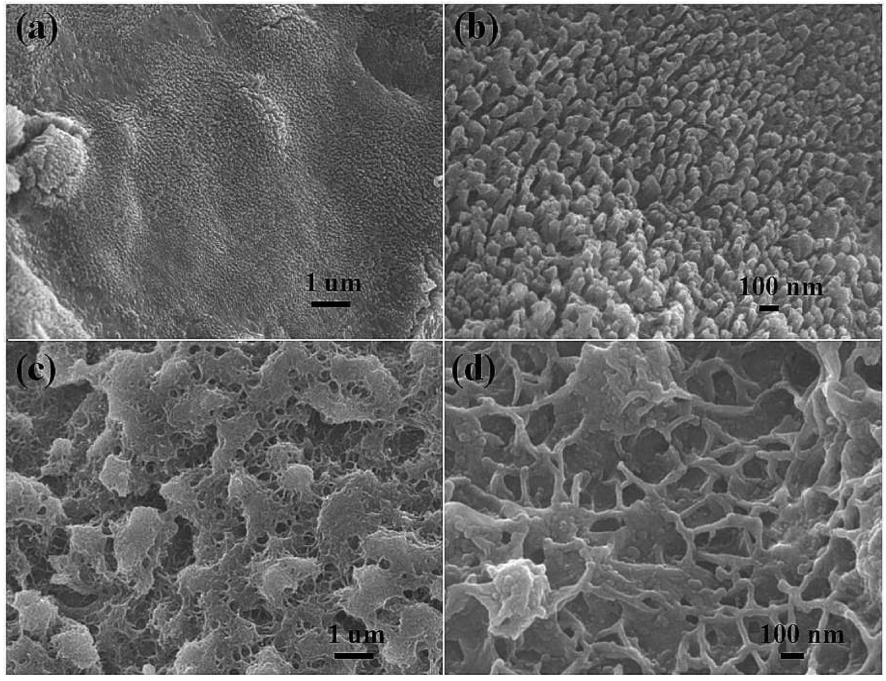

Figure 4. SEM and magnified SEM images of the Pt/CNTs-NF electrode at different D−C stages: (a and b) after the 21th discharging state at 160 mA/g with a restricting capacity of 800 mAh/g and (c and d) after the 86th discharging state at 400 mA/g with a restricting capacity of 1500 mAh/g.

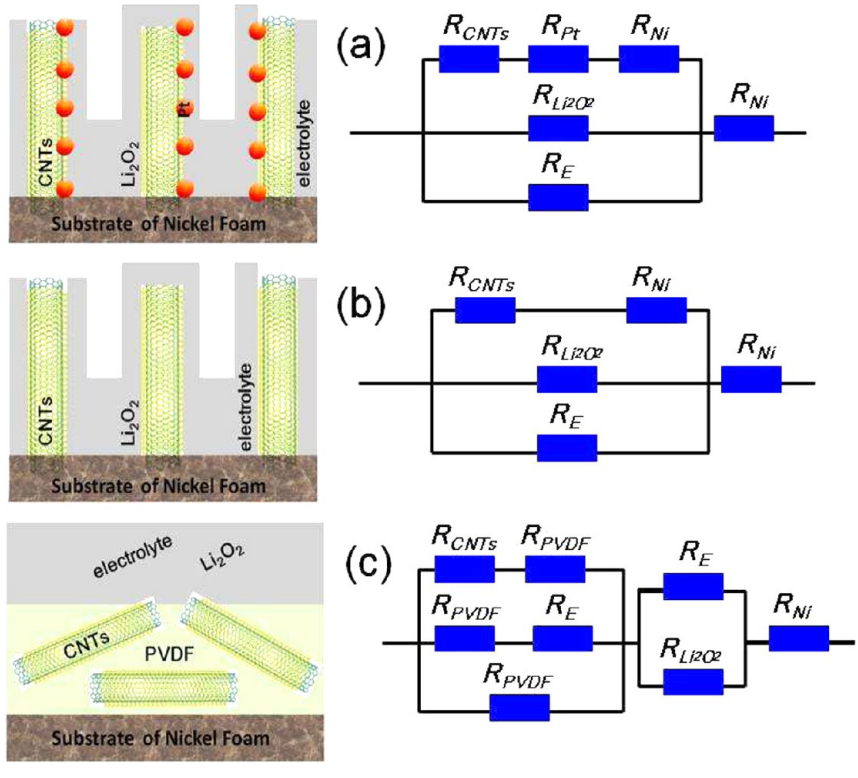

Figure 5. Phenomenological resistance models and corresponding equivalent circuits for (a) the Pt/CNTs-NF electrode, (b) the CNTs-NF electrode, and (c) the CNT-coated electrode.

Accordingly, the EIS results for Pt/CNTs-NF, CNTs-NF, and CNT-coated electrodes before and after long D−C cycles are shown in panels c and f of Figure S15 of the Supporting Information. On the basis of their corresponding equivalent circuit shown in Figure S15f of the Supporting Information,[1,44] the ohmic resistance (R_s) for the CNTs-NF and CNT-coated electrodes remained at 58 and 55 Ω before cycling, respectively, and then increased after long cycling to 338 and 312 Ω, respectively. On the other hand, the R_s for the electrode containing the catalyst of Pt NPs delivered only a small increase from 33 to 72 Ω. In addition, the charge transfer resistance (R_{ct}) of the CNTs-NF or CNT-coated electrode was larger than that of the Pt/CNTs-NF electrode.

For practical application, the electrochemical mechanism in direct current mode for these LOBs should be used. According to scattering theory of the transport of an electron across the interface,[45] Figure 5 compares the phenomenological resistance models and corresponding equivalent circuits for Pt/CNTs-NF, CNTs-NF, and CNT-coated electrodes. Herein, Figure 5 includes carbon (CNTs) resistance R_c, nickel foam resistance R_{Ni}, PVDF resistance R_{PVDF}, Pt resistance R_{Pt}, Li_2O_2 resistance $R_{Li_2O_2}$, and the R_E for resistance arising from electrolyte. The presence of binder PVDF run through the CNT-coated electrode will lead to the obvious increase in total resistance. Meanwhile, the improvement in the conductivity in the Pt/CNTs-NF or CNTs-NF electrode can slow their interface polarization, which is also considered to be responsible for the enhanced electrochemical performance.

CONCLUSION

In summary, an effective integrated design and manufacturing process has been developed for the CNT-based cathodes to improve the performance of the LOBs. The synergistic effect of the unique binder-free architecture of the Pt/CNTs-NF electrode coupled with the high catalytic activity of Pt NPs endows the LOBs with a high specific capacity, superior rate capability, and good cycle stability. This kind of CNT-based electrode coated with another catalyst (e.g., Au, Pd, and Ru) could attract great interest as a potential cathode in LOBs. Meanwhile, enormous scientific and technological challenges to the development of practical devices remain.

ASSOCIATED CONTENT

Supporting Information

SEM and TEM images, SAED Raman and EDS patterns, CV curves, discharge curves, XPS test, and electrochemical impedance spectra. This material is available free of charge via the Internet at http://pubs.acs.org.

AUTHOR INFORMATION

Corresponding Authors

*Telephone and fax: 86-591-83792835. E-mail: guanlh@fjirsm.ac.cn.

*E-mail: zghuang@fjnu.edu.cn.

Notes

The authors declare no competing financial interest.

ACKNOWLEDGMENTS

We acknowledge the financial support by the Natural Science Foundation of China (21203025 and 91127020), the Strategic Priority Research Program of the Chinese Academy of Sciences (Grant XDA09010400), and the National Key Project on Basic Research (Grant 2011CB935904).

REFERENCES

(1) Kitaura, H.; Zhou, H. Electrochemical Performance of Solid-State Lithium-Air Batteries Using Carbon Nanotube Catalyst in the Air Electrode. *Adv. Energy Mater.* **2012**, *2*, 889−894.

(2) Li, J.; Wang, N.; Zhao, Y.; Ding, Y.; Guan, L. MnO_2 Nanoflakes Coated on Multi-Walled Carbon Nanotubes for Rechargeable Lithium-Air Batteries. *Electrochem. Commun.* **2011**, *13*, 698−700.

(3) Chen, Y.; Freunberger, S. A.; Peng, Z.; Fontaine, O.; Bruce, P. G. Charging a Li-O_2 Battery Using a Redox Mediator. *Nat. Chem.* **2013**, *5*, 489−494.

(4) Ottakam Thotiyl, M. M.; Freunberger, S. A.; Peng, Z.; Bruce, P. G. The Carbon Electrode in Nonaqueous Li-O_2 Cells. *J. Am. Chem. Soc.* **2013**, *135*, 494−500.

(5) Gallant, B. M.; Mitchell, R. R.; Kwabi, D. G.; Zhou, J.; Zuin, L.; Thompson, C. V.; Shao-Horn, Y. Chemical and Morphological Changes of Li-O_2 Battery Electrodes upon Cycling. *J. Phys. Chem. C* **2012**, *116*, 20800−20805.

(6) Park, M.; Sun, H.; Lee, H.; Lee, J.; Cho, J. Lithium-Air Batteries: Survey on the Current Status and Perspectives Towards Automotive Applications from a Battery Industry Standpoint. *Adv. Energy Mater.* **2012**, *2*, 780−800.

(7) Black, R.; Adams, B.; Nazar, L. F. Non-Aqueous and Hybrid Li-O_2 Batteries. *Adv. Energy Mater.* **2012**, *2*, 801−815.

(8) Wang, Z. L.; Xu, D.; Xu, J. J.; Zhang, X. B. Oxygen Electrocatalysts in Metal-Air Batteries: From Aqueous to Nonaqueous Electrolytes. *Chem. Soc. Rev.* **2014**, DOI: 10.1039/C3CS60248F.

(9) Mi, R.; Liu, H.; Wang, H.; Wong, K.-W.; Mei, J.; Chen, Y.; Lau, W.-M.; Yan, H. Effects of Nitrogen-Doped Carbon Nanotubes on the Discharge Performance of Li-Air Batteries. *Carbon* **2014**, *67*, 744−752.

(10) Wu, G.; Mack, N. H.; Gao, W.; Ma, S.; Zhong, R.; Han, J.; Baldwin, J. K.; Zelenay, P. Nitrogen-Doped Graphene-Rich Catalysts Derived from Heteroatom Polymers for Oxygen Reduction in Nonaqueous Lithium-O_2 Battery Cathodes. *ACS Nano* **2012**, *6*, 9764−9776.

(11) Truong, T. T.; Liu, Y.; Ren, Y.; Trahey, L.; Sun, Y. Morphological and Crystalline Evolution of Nanostructured MnO_2 and Its Application in Lithium-Air Batteries. *ACS Nano* **2012**, *6*, 8067−8077.

(12) Sun, B.; Zhang, J.; Munroe, P.; Ahn, H.-J.; Wang, G. Hierarchical $NiCo_2O_4$ Nanorods as an Efficient Cathode Catalyst for Rechargeable Non-aqueous Li-O_2 Batteries. *Electrochem. Commun.* **2013**, *31*, 88−91.

(13) Ryu, W. H.; Yoon, T. H.; Song, S. H.; Jeon, S.; Park, Y. J.; Kim, I. D. Bifunctional Composite Catalysts Using Co_3O_4 Nanofibers Immobilized on Nonoxidized Graphene Nanoflakes for High-Capacity and Long-Cycle Li-O_2 Batteries. *Nano Lett.* **2013**, *13*, 4190−4197.

(14) Zhang, K.; Zhang, L.; Chen, X.; He, X.; Wang, X.; Dong, S.; Gu, L.; Liu, Z.; Huang, C.; Cui, G. Molybdenum Nitride/N-doped Carbon Nanospheres for Lithium-O_2 Battery Cathode Electrocatalyst. *ACS Appl. Mater. Interfaces* **2013**, *5*, 3677−3682.

(15) Dong, S.; Chen, X.; Wang, S.; Gu, L.; Zhang, L.; Wang, X.; Zhou, X.; Liu, Z.; Han, P.; Duan, Y.; Xu, H.; Yao, J.; Zhang, C.; Zhang, K.; Cui, G.; Chen, L. 1D Coaxial Platinum/Titanium Nitride Nanotube Arrays with Enhanced Electrocatalytic Activity for the Oxygen Reduction Reaction: Towards Li-Air Batteries. *ChemSusChem* **2012**, *5*, 1712−1715.

(16) Oh, S. H.; Nazar, L. F. Oxide Catalysts for Rechargeable High-Capacity Li-O_2 Batteries. *Adv. Energy Mater.* **2012**, *2*, 903−910.

(17) Shen, Y.; Sun, D.; Yu, L.; Zhang, W.; Shang, Y.; Tang, H.; Wu, J.; Cao, A.; Huang, Y. A High-Capacity Lithium-Air Battery with Pd Modified Carbon Nanotube Sponge Cathode Working in Regular Air. *Carbon* **2013**, *62*, 288−295.

(18) Lu, Y. C.; Kwabi, D. G.; Yao, K. P. C.; Harding, J. R.; Zhou, J.; Zuin, L.; Shao-Horn, Y. The discharge rate capability of rechargeable Li-O_2 batteries. *Energy Environ. Sci.* **2011**, *4*, 2999.

(19) Xu, J. J.; Xu, D.; Wang, Z. L.; Wang, H. G.; Zhang, L. L.; Zhang, X. B. Synthesis of Perovskite-Based Porous $La_{0.75}Sr_{0.25}MnO_3$ Nanotubes as A Highly Efficient Electrocatalyst for Rechargeable Lithium-Oxygen Batteries. *Angew. Chem., Int. Ed.* **2013**, *52*, 3887−3890.

(20) Shui, J. L.; Karan, N. K.; Balasubramanian, M.; Li, S. Y.; Liu, D. J. Fe/N/C Composite in Li-O_2 Battery: Studies of Catalytic Structure and Activity Toward Oxygen Evolution Reaction. *J. Am. Chem. Soc.* **2012**, *134*, 16654−16661.

(21) Zhang, K.; Zhang, L.; Chen, X.; He, X.; Wang, X.; Dong, S.; Han, P.; Zhang, C.; Wang, S.; Gu, L.; Cui, G. Mesoporous Cobalt Molybdenum Nitride: A Highly Active Bifunctional Electrocatalyst and Its Application in Lithium-O_2 Batteries. *J. Phys. Chem. C* **2013**, *117*, 858−865.

(22) Ottakam Thotiyl, M. M.; Freunberger, S. A.; Peng, Z.; Chen, Y.; Liu, Z.; Bruce, P. G. A Stable Cathode for the Aprotic Li-O_2 Battery. *Nat. Mater.* **2013**, *12*, 1050−1056.
(23) Lu, Y.; Wen, Z.; Jin, J.; Cui, Y.; Wu, M.; Sun, S. Mesoporous Carbon Nitride Loaded with Pt Nanoparticles as a Bifunctional Air Electrode for Rechargeable Lithium-Air Battery. *J. Solid State Electrochem.* **2012**, *16*, 1863−1868.
(24) Lu, Y.-C.; Xu, Z.; Gasteiger, H. A.; Chen, S.; Hamad-Schifferli, K.; Shao-Horn, Y. Platinum-Gold Nanoparticles: A Highly Active Bifunctional Electrocatalyst for Rechargeable Lithium-Air Batteries. *J. Am. Chem. Soc.* **2010**, *132*, 12170−12171.
(25) Yang, Y.; Shi, M.; Zhou, Q.-F.; Li, Y.-S.; Fu, Z.-W. Platinum Nanoparticle-Graphene Hybrids Synthesized by Liquid Phase Pulsed Laser Ablation as Cathode Catalysts for Li-Air Batteries. *Electrochem. Commun.* **2012**, *20*, 11−14.
(26) Yilmaz, E.; Yogi, C.; Yamanaka, K.; Ohta, T.; Byon, H. R. Promoting Formation of Noncrystalline Li_2O_2 in the Li-O_2 Battery with RuO_2 Nanoparticles. *Nano Lett.* **2013**, *13*, 4679−4684.
(27) Cheng, F.; Chen, J. Metal-Air Batteries: From Oxygen Reduction Electrochemistry to Cathode Catalysts. *Chem. Soc. Rev.* **2012**, *41*, 2172−2192.
(28) Jung, H.-G.; Jeong, Y. S.; Park, J.-B.; Sun, Y.-K.; Scrosati, B.; Lee, Y. J. Ruthenium-Based Electrocatalysts Supported on Reduced Graphene Oxide for Lithium-Air Batteries. *ACS Nano* **2013**, *7*, 3532−3539.
(29) Tran, C.; Yang, X.-Q.; Qu, D. Investigation of the Gas-Diffusion-Electrode Used as Lithium/Air Cathode in Non-Aqueous Electrolyte and the Importance of Carbon Material Porosity. *J. Power Sources* **2010**, *195*, 2057−2063.
(30) Zhang, G. Q.; Zheng, J. P.; Liang, R.; Zhang, C.; Wang, B.; Hendrickson, M.; Plichta, E. J. Lithium-Air Batteries Using SWNT/CNF Buckypapers as Air Electrodes. *J. Electrochem. Soc.* **2010**, *157*, A953−A956.
(31) Zhang, W.; Zhu, J.; Ang, H.; Zeng, Y.; Xiao, N.; Gao, Y.; Liu, W.; Hng, H. H.; Yan, Q. Binder-Free Graphene Foams for O_2 Electrodes of Li-O_2 Batteries. *Nanoscale* **2013**, *5*, 9651−9658.
(32) Lin, X.; Lu, X.; Huang, T.; Liu, Z.; Yu, A. Binder-Free Nitrogen-Doped Carbon Nanotubes Electrodes for Lithium-Oxygen Batteries. *J. Power Sources* **2013**, *242*, 855−859.
(33) Mitchell, R. R.; Gallant, B. M.; Thompson, C. V.; Shao-Horn, Y. All-Carbon-Nanofiber Electrodes for High-Energy Rechargeable Li-O_2 Batteries. *Energy Environ. Sci.* **2011**, *4*, 2952−2958.
(34) McCloskey, B. D.; Bethune, D. S.; Shelby, R. M.; Girishkumar, G.; Luntz, A. C. Solvents' Critical Role in Nonaqueous Lithium-Oxygen Battery Electrochemistry. *J. Phys. Chem. Lett.* **2011**, *2*, 1161−1166.
(35) Li, L.; Meng, F.; Jin, S. High-Capacity Lithium-Ion Battery Conversion Cathodes Based on Iron Fluoride Nanowires and Insights into the Conversion Mechanism. *Nano Lett.* **2012**, *12*, 6030−6037.
(36) Su, D.; Kim, H.-S.; Kim, W.-S.; Wang, G. A Study of PtxCoy Alloy Nanoparticles as Cathode Catalysts for Lithium-Air Batteries with Improved Catalytic Activity. *J. Power Sources* **2013**, *244*, 488−493.
(37) Wang, L.; Ara, M.; Wadumesthrige, K.; Salley, S.; Ng, K. Y. S. Graphene Nanosheet Supported Bifunctional Catalyst for High Cycle Life Li-Air Batteries. *J. Power Sources* **2013**, *234*, 8−15.
(38) Cheng, H.; Scott, K. Selection of Oxygen Reduction Catalysts for Rechargeable Lithium-Air batteries-Metal or Oxide? *Appl. Catal., B* **2011**, *108−109*, 140−151.
(39) Ko, B. K.; Kim, M. K.; Kim, S. H.; Lee, M. A.; Shim, S. E.; Baeck, S.-H. Synthesis and Electrocatalytic Properties of Various Metals Supported on Carbon for Lithium-Air Battery. *J. Mol. Catal. A: Chem.* **2013**, *379*, 9−14.
(40) Yin, J.; Fang, B.; Luo, J.; Wanjala, B.; Mott, D.; Loukrakpam, R.; Ng, M. S.; Li, Z.; Hong, J.; Whittingham, M. S.; Zhong, C.-J. Nanoscale Alloying Effect of Gold-Platinum Nanoparticles as Cathode Catalysts on the Performance of a Rechargeable Lithium-Oxygen Battery. *Nanotechnology* **2012**, *23* (30), 305404−305411.
(41) Lu, Y.-C.; Crumlin, E. J.; Carney, T. J.; Baggetto, L.; Veith, G. M.; Dudney, N. J.; Liu, Z.; Shao-Horn, Y. Influence of Hydrocarbon and CO_2 on the Reversibility of Li-O_2 Chemistry Using *In Situ* Ambient Pressure X-ray Photoelectron Spectroscopy. *J. Phys. Chem. C* **2013**, *117* (49), 25948−25954.
(42) Li, F.; Tang, D.-M.; Chen, Y.; Golberg, D.; Kitaura, H.; Zhang, T.; Yamada, A.; Zhou, H. Ru/ITO: A Carbon-Free Cathode for Nonaqueous Li-O_2 Battery. *Nano Lett.* **2013**, *13* (10), 4702−4707.
(43) Freunberger, S. A.; Chen, Y.; Drewett, N. E.; Hardwick, L. J.; Bardé, F.; Bruce, P. G. The Lithium-Oxygen Battery with Ether-Based Electrolytes. *Angew. Chem., Int. Ed.* **2011**, *50*, 8609−8613.
(44) Kichambare, P.; Kumar, J.; Rodrigues, S.; Kumar, B. Electrochemical Performance of Highly Mesoporous Nitrogen Doped Carbon Cathode in Lithium-Oxygen Batteries. *J. Power Sources* **2011**, *196*, 3310−3316.
(45) Huang, Z.; Chen, Z.; Peng, K.; Wang, D.; Zhang, F.; Zhang, W.; Du, Y. Monte Carlo Simulation of Tunneling Magnetoresistance in Nanostructured Materials. *Phys. Rev. B* **2004**, *69* (9), 094420−094427.